Thermal decomposition of [LiNb($OC_6H_3Me_2$-2,4)$_6$] as potential single source molecular precursor $LiNbO_3$ nanopowder: Structural and dielectric studies

Manjula Sharma* and Neeraj Sharma

Department of Chemistry, Himachal Pradesh University, Summer Hill, Shimla-171005, India

E-mail: manjula.angiras19@gmail.com

*https://orcid.org/0000-0001-6626-7136

Abstract: The new heterometallic lithium-niobium aryloxide of composition [LiNb($OC_6H_3Me_2$-2,4)$_6$] has been synthesized by the reaction of [Nb($OC_6H_3Me_2$-2,4)$_5$] with equimolar amount of [$LiOC_6H_3Me_2$-2,4] in dry benzene and characterized by physicochemical and IR and ^{1}H NMR spectral studies. Thermal behaviour of complex studied by TG-DTA techniques in air has yielded pure, single phase $LiNbO_3$ at 684.56^{o}C and characterized by Fourier transform infrared spectroscopy (FTIR), X-ray powder diffraction (XRD) and Scanning electron microscopy (SEM). The XRD pattern of $LiNbO_3$ nanopowder has revealed a trigonal crystalline phase with average crystallite size of 54nm. SEM micrographs have shown uniform shape with spherical morphology. The dielectric properties viz. dielectric constant (ε) and dielectric loss (tan δ) of as obtained $LiNbO_3$ nanopowder have been studied as a function of frequency in 1kHz-1MHz range at room temperature. The variation of both the parameters ε and tan δ has also been examined as a function of temperature in 50-350^{o}C range at different frequencies (1kHz-1MHz). The observed trends of decrease in ε as well as tan δ with increase in frequency and increase with rise in temperature have established the diagnostic characteristics of dielectric behaviour of studied $LiNbO_3$ nanopowder.

Key Words: [$LiNb(OC_6H_3Me_2\text{-}2,4)_6$], thermal decomposition, dielectric properties, $LiNbO_3$

1. Introduction:

Lithium niobate ($LiNbO_3$, LN) a ferroelectric compound as monocrystals/ nanocrystals/ nanopowders/ microfibers/ thin films has drawn immense research interest due to its numerous dielectric, electro-optic, ferroelectric, piezoelectric properties [1-6]. They find utility in optical devices, microelectronic circuits, pyroelectric detectors, second harmonic generation surface acoustic wave devices, holographic memory, modulators etc [7-11]. As characteristics of the materials are strongly influenced by preparative methods, $LiNbO_3$ powders have been reported to be prepared by conventional high temperature processes such as single-crystal Czochralski growth [12], capillary liquid epitaxial technique [13], Stepanov growth [14], laser-heated pedestrial growth [15], sol-gel [16], Pechini method [17], amine assisted method [18], hydrothermal synthesis [19], wet chemical method [20], polymeric precursor method [21], solvothermal method [22] etc. The control of the stoichiometry, size and homogeneity during preparation process is highly desirable in all the methods. The conventional solid-state method involves high cost and time and temperature above 1200°C resulting in the evaporation of lithium content and formation of non-stoichiometric product [23]. Literature reveals that metal alkoxides have been recognised as versatile potential candidates for functional inorganic materials because of their mechanical, electronic and optical properties of utility in material science. The new insight in the role of modifying ligands in the sol-gel processing of metal alkoxide precursors as a possibility to approach new classes of materials has been reported [24]. The synthesis, structural principles and reactivity of heterometallic alkoxides, multicomponent oxides have also been extensively

investigated owing to their enormous importance as potential molecular precursors. The stoichiometric $LiNbO_3$ crystal, with an equal molar ratio of Li and Nb, hmas interesting properties and is beneficial in many applications, because ost of its useful qualities are dependent on the Li/Nb ratio [25,26]. Hence the synthesis and structural characterization of dimeric molecular precursor has been reported for the preparation of lithium niobate powders by their controlled partial hydrolysis. The synthesis of novel lithium-niobium(V) oxoaryloxide $LiNbO(O\text{-}2,6\text{-}PhMe_2)_4.3THF$ as monomeric binuclear complex and lithium-niobium(V) chlorido aryloxide $[LiNbCl_3(O\text{-}2,6\text{-}PhMe_2)_2.2THF]_2$ as dimeric tetranuclear complex by methathesis reaction of $NbCl_5$ with lithium-2,6-dimethylphenoxide $LiO\text{-}2,6\text{-}PhMe_2$ in THF at room temperature has been reported [27] The use of niobium alkoxides for the production of mixed-metal oxide thin films materials has also been reported [28]. The synthesis of lithium niobium complexes without any intermolecular bonds or bridging units has been reported by the incorporation of bulky aryl groups viz. methyl side chains at aromatic ring [29]. Despite the fact that numerous reports describe the preparation, characterization and potential applications of $LiNbO_3$, there is continuous search for new improved precursors, simple preparative methods and fascinating properties in material science. In continuation of our interest on niobium aryloxides [30-34] we herein report the synthesis and characterization of new heterometallic lithium niobium aryloxide $[LiNb(OC_6H_3Me_2\text{-}2,4)_6]$ and its exploration as single-source precursor to lithium niobate nanopowder by TG-DTA techniques. The FT-IR, XRD and SEM methods have established the formation of $LiNbO_3$. The dielectric properties of as obtained $LiNbO_3$ have also been studied.

2. Experimental

2.1 Materials and methods

The reagent grade solvents were distilled and dried by standard methods before use. Niobium pentachloride (Fluka) was used without further purification; however, its purity was checked by chlorine analysis. 2,4-Dimethylphenol (B.pt. 25-26°C, Merck) and lithium metal (Merck) were used. The niobium content in complex was estimated as Nb_2O_5 after decomposing it with a mixture of conc. H_2SO_4 and HNO_3 followed by heating at 650-700 °C. Micro-analyses for carbon and hydrogen were performed on Eager 300 NCH System Elemental Analyzer. The molecular weight was determined cryoscopically in benzene (0.0015-0.0020 M) using a Beckmann thermometer. Infrared spectra were recorded (KBr pellets) on Nicolet-5700 FTIR Spectrometer. ^1H NMR spectra was recorded on BRUKERAVANCE II 400 Spectrometer using TMS as an internal standard and $CDCl_3$ as solvent. The thermal behaviour of heterometallic aryloxide was studied by TG-DTA techniques on NETZSCH Geratebau GmbH TG-DTA thermal analyzer in an air atmosphere at a heating rate of 10°C/ min from room temperature to 800°C. The phase identification and structure analysis of $LiNbO_3$ powders were carried out by X-ray diffraction (XRD) on Philips X-ray diffractometer (Model PW 3071 X'Pert PRO') equipped with Cu-*K*α radiation (λ*=1.5416 Å)* from 2θ = 20° to 70°. The microstructure and morphology analyses were carried out on 'FEI Quanta 250' scanning electron microscope operating at 20kV. The LN powder was pressed into round pellet on KBr hydraulic press at a pressure of 3 tons and 9mm in diameter and 2mm in thickness. It was sintered at 700°C. The pellet was polished and surfaces were made flat, electrode with dry conducting silver paste and dried at 150°C for 1h to remove moisture. It was then cooled to room temperature. The dielectric

properties of LN nanopowder were measured as a function of frequency and temperature on an LCR meter (PSM 1735).

2.2. Synthesis of [Nb($OC_6H_3Me_2$-2,4)$_5$]

The synthetic procedure for [Nb($OC_6H_3(CH_3)_2$-2,4)$_5$] has been published previously by us.[29]

2.3. Synthesis of [Li($OC_6H_3Me_2$-2,4)]

The lithium salt of 2, 4-dimethylphenol was prepared by the reaction of fine cut lithium metal (1g; 0.14mol) with an equimolar amount of 2,4-dimethylphenol (17.4g; 0.14mol) in benzene at room temperature. The contents were stirred for 5-6 h during which the separation of white solid was observed. It was filtered under anhydrous conditions, washed 2-3 times with dry benzene and finally dried under vacuum. Yield 86%. Anal. Calcd. for **C_8H_9OLi** /128 (%): C, 75.00; H, 7.03. Found (%): C, 74.46; H, 6.94.

2.4. Synthesis of [LiNb($OC_6H_3Me_2$-2,4)$_6$]

In a typical reaction, to a suspension of [Nb($OC_6H_3(CH_3)_2$-2,4)$_5$] (3.62g; 0.0052 mol) in dry benzene was added a suspension of [Li($OC_6H_3(CH_3)_2$-2,4)] (0.66g, 0.0052 mol) in the same solvent. The reaction mixture was initially stirred and then refluxed for 24 h. The addition of petroleum ether gave dark brown powder and was dried under vacuum. It was recrystallized from benzene. Yield 78%. Anal. Calcd. for **$C_{48}H_{54}O_6NbLi$** /826 (%): C, 69.73; H, 6.53; Nb, 11.26. Found (%): C, 69.46; H, 6.24; Nb, 11.14. $\wedge_{m,}$ ($PhNO_2$): 7.68 Scm^2M^{-1}. IR (KBr, cm^{-1}): 3028, 2964, 2858, 1548, 1479, 1354, 1275, 1240, 1151, 1127, 1071, 1033, 894, 755, 698, 611, 556, 552. ^{1}H NMR (400 MHz, $CDCl_3$, ppm): δ7.28(s, 6H, ArH-3), δ7.14(d, 6H, ArH-5), δ6.99(d, 6H, ArH-6), δ2.43(s, 18H, $ArCH_3$-2), δ2.87(s, 18H, $ArCH_3$-4).

3. RESULTS AND DISCUSSION

The reaction of $[Nb(OC_6H_3Me_2\text{-}2,4)_5]$ with $[Li(OC_6H_3Me_2\text{-}2,4)]$ in 1:1 molar ratio in benzene under reflux has led to the formation of dark brown heterometallic aryloxide in conformity with elemental analyses according to the equation:

$$[Nb(OC_6H_3(CH_3)_2\text{-}2,4)_5] + Li(OC_6H_3(CH_3)_2\text{-}2,4) \xrightarrow{\text{Benzene}} [LiNb(OC_6H_3(CH_3)_2\text{-}2,4)_6]$$

Scheme 1. Synthesis of $[LiNb(OC_6H_3Me_2\text{-}2,4)_6]$

The complex is quite stable in dry air and appreciably soluble in benzene, nitrobenzene and chloroform. The molar conductance value (7.68 Scm^2mol^{-1}) of the millimolar solution of complex in nitrobenzene has indicated its appreciable electrolytic nature relative to parent pentaaryloxide $[Nb(OC_6H_3(CH_3)_2\text{-}2,4)_5]$ (0.37 Scm^2mol^{-1}).

3.1. IR Spectra

The formation of heterometallic complex has been established from a comparison of its FTIR spectra with that of $[Nb(OC_6H_3Me_2\text{-}2,4)_5]$ recorded in 4000-400 cm^{-1} region. The υ(C−O) mode has been found to shift towards higher region by 15-20 cm^{-1} for $Li[Nb(OC_6H_3Me_2\text{-}2,4)_6]$ and occurred at 1275-1240 cm^{-1} range relative to $[Nb(OC_6H_3Me_2\text{-}2,4)_5]$ (1260-1220 cm^{-1}) which may be attributed to the fact that the negative charge existing on metal in $[Nb(OC_6H_3Me_2\text{-}2,4)_6]^-$ decreases the drainage of electron density from the ring to the metal thereby, strengthening the C−O bond and resultant higher frequencies for the υ(C−O) mode. The bands appeared at 1151 cm^{-1} and 1127 cm^{-1} have been ascribed to υ(Li–O) mode. The bands at 552 cm^{-1} and 556 cm^{-1} have been assigned to υ(Nb−O) vibrations.

3.2. ^{1}H NMR Spectra

The ^{1}H NMR spectrum of $[LiNb(OC_6H_3Me_2\text{-}2,4)_6]$ displayed signals in δ6.99-7.28 ppm and δ2.43-2.87 ppm range due to phenolic ring protons and methyl substituents

respectively shifted downfield relative to those occurred at δ6.81-6.64 and δ2.08-2.20 in [Nb($OC_6H_3Me_2$-2,4)$_5$].

3.3. Thermal Studies

The TG curve of Li[Nb($OC_6H_3Me_2$-2,4)$_6$] (Figure 1) recorded in air has shown it to be thermally stable upto 55ºC after which temperature a continuous single stage decomposition is indicated by the non-observance of any plateau in TG curve thereby excluding the possibility of formation of any intermediate. The experimental mass loss of 82.78% as compared to calculated 82.12% in 55-685°C range has accounted for the formation of $LiNbO_3$ as the pale yellow decomposition product indicating that temperature for Li[Nb($OC_6H_3Me_2$-2,4)$_6$] precursor to obtain quality $LiNbO_3$ powder is 685ºC. It is pertinent to maintain here that heat treatment at temperature above 500 ºC has reported to promote the formation of LN crystals and increase in the particle size [35]. The formation of LN polycrystalline phase has been reported to be formed directly from the thermal decomposition of the precursor gel by heat treatment at 600ºC for 2 hr [36]. The DTA curve of [LiNb($OC_6H_3Me_2$-2,4)$_6$] has shown two exothermic peaks at 446ºC and 558ºC assigned to combustion of organic species.

3.4 Characterization of $LiNbO_3$ powder

An accelerating research interest has been drawn in processing of materials in nanometer and micrometer scales owing to their diverse potential applications associated with size, geometry and morphology. The development of molecular precursors has largely increased over the years and numerous synthetic strategies have evolved for $LiNbO_3$ nanopowder (Table 1).

3.4.1. IR Spectra

The IR spectrum of as obtained $LiNbO_3$ nanopowder (Figure 2) has shown an absorption band at 570 cm^{-1} assigned to Nb–O vibration in crystal structure [49]. The bands due to Li–O vibrations have appeared at 1117 cm^{-1} and 1128 cm^{-1}. The non-observance of absorption bands due to ν(C–O) mode occurred in precursor has substantiated the formation of $LiNbO_3$ nanopowder.

3.4.2. XRD Spectra

The X-ray diffraction (XRD) pattern of $LiNbO_3$ in Figure 3. has shown the major peaks indexed as 012, 104, 110, 006, 113 and 202 and no reflection peaks assignable to Li_2O, Nb_2O_5, $LiNb_3O_8$ or other second phase appeared. The crystalline phase of $LiNbO_3$ nanopowder has been assigned as a trigonal, in agreement with the previously reported data (ICCD Card File No. 20-361). The average crystallite size has been calculated using Scherrer equation [50]:

$$\tau = \frac{K\lambda}{\beta cos\theta}$$

where τ is the mean size of the ordered (crystalline) domains, smaller or equal to grain size, K a dimensionless shape factor with a value close to unity i.e. typical value of ~0.9 but varies with actual shape of the crystallite, λ the wavelength of incident ray (1.5418 Å), β the full width at half the maximum intensity (FWHM) and θ Bragg's diffraction angle. The particle size has been found to be 54 nm.

3.4.3. SEM

SEM images were acquired in order to understand the morphology of the $LiNbO_3$ particles. These images exhibits highly agglomerated particles having some voids. Images also show that the particles have cluster-like nanostructures with non-uniform

size distribution. A representative SEM image of $LiNbO_3$ particles is depicted in Figure 4. ImageJ software [51] provided further insight into the particle size distribution profile of the $LiNbO_3$ particles and average particle size has been found to be 98 nm (Figure 5).

3.4.4. Dielectric properties

A few scattered reports are available on the dielectric properties of significantly important $LiNbO_3$ nanopowders of technological potential. The dielectric constant (ε) and dielectric loss (tanδ) factors usually determine the suitability of a particular material for electronic applications. Dielectric responses result from the short-range motion of charge carriers under the influence of applied electric field. The electrical energy upon applying a.c. voltage is absorbed by the dielectric which may be dissipated in the form of heat termed as dielectric loss. The displacement of charge leads to the storage of electrical energy which is the capacitance of the dielectric. The capacitance of flat, parallel metallic plates of area A and distance between the plates d is given by the expression:

$$C = \frac{\varepsilon A}{d} = \frac{k\varepsilon_o A}{d}$$

where ε_o is the permittivity of free space (8.854×10^{-12} F/m)

k = relative permittivity of the dielectric material and for free space k = 1

For a dielectric material, an oscillating field ($E = E_o e^{i\omega t}$) and the displacement field ($D = D_o e^{j(\omega t - \delta)}$) lead to a complex quantity as

$$\frac{D_o}{E_o} e^{-j\delta} = \varepsilon_r^{'} - j\varepsilon_r^{''} = \varepsilon_r^{*}$$

where the relative permitivity or dielectric constant $\varepsilon_r^{'} = \frac{D_o}{E_o}\cos\delta$ and dielectric loss $\varepsilon_r^{'} = \frac{D_o}{E_o}\sin\delta$ and $tan\delta = \frac{\varepsilon_r^{''}}{\varepsilon_r^{'}}$ is called loss tangent or dissipation of the dielectric indicating the amount of energy that is dissipated in the dielectric when an electric field is applied across it.

Literature reports that conduction in nanocrystalline LN may result from oxygen vacancies, low pressure (<1 atm), lithium ions in high pressure conditions and Li/Nb ratio both for low and high pressure [52]. The frequency dependence of dielectric constant (ε) and variation of loss tangent or dissipation (tanδ) at room temperature in Figure 6 has shown that both the parameters have been found to decrease with increase in frequency indicating a normal behavior of dielectric material at room temperature [53] The variation of dielectric constant (ε) of $LiNbO_3$ nanopowder as a function of temperature at different frequencies (Figure 7) has shown that dielectric constant (ε) first decreases and later increases with increasing temperature for frequency range 1kHz-100kHz. For frequency 1000kHz the dielectric constant values has been found to decrease with increase in temperature. The high dielectric constant at low frequencies may be attributed to polarization effects at the electrode-electrolyte interface with the presence of Li^+ ion hopping conduction [54,55] The variation of loss tangent (tanδ) as a function of temperature at different frequencies (1kHz-1MHz) (Figure 8) seems to follow the behaviour similar to that of dielectric constant i.e. increase of tanδ with rise in temperature which may be ascribed to the enhancement in conductivity [56,57]. The low dielectric loss for a given sample at high frequency suggests superior optical quality with lower flaws and this parameter plays an important role in nonlinear optical

materials. The rapid increase of loss tangent (tanδ) at high temperature in low frequency region may be attributed to space charge polarization.

4. Conclusions

The new heterometallic lithium-niobium aryloxide [$LiNb(OC_6H_3Me_2\text{-}2,4)_6$] has been synthesized and characterized. Thermal decomposition of complex studied by thermogravimetric technique in air has yielded $LiNbO_3$ as decomposition product at 684.54 ^oC. XRD pattern of as obtained $LiNbO_3$ has shown trigonal crystalline phase with average crystallite size of 54nm. The uniform shape with spherical morphology has been inferred from SEM. The dielectric studies of $LiNbO_3$ nanopowder have revealed that both the dielectric constant (ε) and dielectric loss (tanδ) decrease with an increase in frequency and increases with rise in temperature which are suggestive of frequency-dependent behaviour. The present work has shown that [$LiNb(OC_6H_3Me_2\text{-}2,4)_6$] finds use as a promising single source molecular precursor to obtain good quality $LiNbO_3$ nanopowder by thermal decomposition method at a reasonably low temperature and reduced cost. The crystallization temperature of $LiNbO_3$ in the current study has been shown to be close to the previously studied lithium niobium aryloxides. It is worth mentioning that $LiNbO_3$ obtained from the non-alkoxide or halide precursors requires significantly higher temperature for the decomposition of the intermediates. The current study deals with the synthesis of lithium nionium aryloxede as single source precursor to LiNbO3 nanopowders, but additional work is required to study the effect of lattice strain and grain size on the dielectric properties - both of which will be subjects of future work.

Acknowledgements

Manjula Sharma is thankful to University Grant Commission (UGC), New Delhi for providing Senior Research Fellowship (UGC-BSR). The authors thank Department of Science and Technology (DST), Government of India, New Delhi for financial assistance for FT-IR facility to the department under its FIST program; Sophisticated Analytical Instrument Facility, Panjab University Chandigarh for recording XRD, ^{1}H NMR and SEM and IIT, Mandi for recording TG-DTA.

References

1. Bergman J G , Ashkin A, Ballman A A, Dziedzic J M, Levitlstein H J et al. Curie temperature, birefringence, and phase-matching temperature variations in $LiNbO_3$ as a function of melt stoichiometry. Applied Physics Letter 1968; 12: 92-94. https://doi.org/10.1063/1.1651912
2. Weis R S and Gaylord T K. Lithium niobate: Summary of physical properties and crystal structure. Applied Physics A 1985; 37(4): 191-203. https://doi.org/10.1007/BF00614817
3. Mohanty D, Chaubey G S, Yourdkhani A, Adireddy S, Caruntu G et al. Synthesis and piezoelectric response of cubic and spherical $LiNbO_3$ nanocrystals. RSC Advances 2012; 2:1913-1916. https://doi.org/10.1039/C2RA00628F
4. Smith R T and Welsh F S. Temperature dependence of the elastic, piezoelectric, and dielectric constants of lithium tantalate and lithium niobate. Journal of Applied Physics 1971; 42(6): 2219-2230. https://doi.org/10.1063/1.1660528
5. Henson R M, Zeyfang R R and Kiehl K V, Dielectric and electromechanical properties of $(Li,Na)NbO_3$ ceramics. Journal of the American Ceramic Society 1977; 60(1–2): 15-17. https://doi.org/10.1111/j.1151-2916.1977.tb16083.x

6. Carville N C, Collins L, Manzo M, Gallo K, Lukasz B I et al. Biocompatibility of ferroelectric lithium niobate and the influence of polarization charge on osteoblast proliferation and function. Journal of Biomedical Materials Research Part A 2015; 103A: 2540-2548. https://doi.org/10.1002/jbm.a.35390
7. Wooten E L, Kissa K M, Yi-Yan A, Murphy E J, Lafaw D A et al. A review of lithium niobate modulators for fiber-optic communications systems. IEEE Journal of selected topics in Quantum Electronics 2000; 6(1): 69-82. https://doi.org/10.1109/2944.826874
8. Lim E J, Fejer M M and Byer R L. Second-harmonic generation of green light in periodically poled planar lithium niobate waveguide. Electronics Letters 1989; 25(3): 174-175. https://doi.org/10.1049/el:19890127
9. Asobe M, Yokohama I, Itoh H, Kaino T. All-optical switching by use of cascading of phase-matched sum-frequency-generation and difference-frequency-generation processes in periodically poled $LiNbO_3$. Optics Letters 1997; 22: 274-276. https://doi.org/10.1364/OL.22.000274
10. Wang Y, Zhou X Y, Chen Z, Cai B, Ye Z Z et al. Synthesis of cubic $LiNbO_3$ nanoparticles and their application in vitro bioimaging. Applied Physics A 2014; 117: 2121-2126. https://doi.org/10.1007/s00339-014-8630-x
11. Sarker M R, Karim H, Martinez R, Love N, Lin Y. A Lithium niobate high-temperature sensor for energy system applications. IEEE Sensors Journal 2016; 16(15): 5883-5888. https://doi.org/10.1109/JSEN.2016.2575399
12. Baumann I, Rudolph P, Krabe D and Schalge R. Orthoscopic investigation of the axial optical and compositional homogeneity of Czochralski grown $LiNbO_3$

crystals. Journal of Crystal Growth 1993; 128: 903-908. https://doi.org/10.1016/S0022-0248(07)80067-4

13. Fukuda T, Hirano H. $LiNbO_3$ and $LiTaO_3$ growth by the capillary liquid epitaxial technique. Journal of Crystal Growth 1980; 50(1): 291-298. https://doi.org/10.1016/0022-0248(80)90251-1

14. Red'kin B S, Kurlov V N, Tatarchenko V A. The stepanov growth of $LiNbO_3$ crystals. Journal of Crystal Growth 1987; 82: 106-109. https://doi.org/10.1016/0022-0248(87)90172-2

15. Luh Y S, Feigelson R S, Fejer M M, Byer R L. Ferroelectric domain structures in $LiNbO_3$ single-crystal fibers. Journal Crystal Growth 1986; 78: 135-143. https://doi.org/10.1016/0022-0248(86)90510-5

16. Wang L H, Yuan D R, Yuan X L, Wang X Q, Yu F P. Synthesis and characterization of fine lithium niobate powders by sol–gel method. Crystal Research and Technology 2007; 42: 321-324. https://doi.org/10.1002/crat.200610822

17. Gracá M P F, Prezas P R, Costa M M, Valente M A. Structural and dielectric characterization of $LiNbO_3$ nano-size powders obtained by Pechini method. Journal of Sol-Gel Science and Technology 2012; 64(10): 78-85. https://doi.org/10.1007/s10971-012-2829-0

18. Liu M, Xue D. Amine-assisted route to fabricate $LiNbO_3$ particles with a tunable shape. Journal of Physical Chemistry C 2008; 112(16): 6346-6351. https://doi.org/10.1021/jp800803s

19. Yu J, Liu X. Hydrothermal synthesis and characterization of $LiNbO_3$ crystal. Materials Letters 2007; 61(2): 355-358. https://doi.org/10.1016/j.matlet.2006.04.087
20. Yao S, Zheng F, Liu H, Wang J, Zhang H. Synthesis of stoichiometric $LiNbO_3$ nanopowder through a wet chemical method. Crystal Research and Technology 2009; 44(11): 1235- 1240. https://doi.org/10.1002/crat.200900064
21. Simões A Z, Zaghete M A, Stojanovic B D, Riccardi C S, Ries A. $LiNbO_3$ thin films prepared through polymeric precursor method. Materials Letters 2003; 57(15): 2333-2339. https://doi.org/10.1016/S0167-577X(02)01221-1
22. Prakash B J and Buddhudu S. Synthesis and analysis of $LiNbO_3$ ceramic powders by co-precipitation method. Indian Journal of Pure Applied Physics 2012; 50(05): 320-324.
23. Caulton K G, Hubert-Pfalzgraf L G. Synthesis, structural principles and reactivity of heterometallic alkoxides. Chemical Reviews 1990; 90(6): 969-995. https://doi.org/10.1021/cr00104a003
24. Eichorst D J, Howard K E, Payne D A, Wilson S R. Crystal structure of lithium niobium ethoxide ($LiNb(OCH_2CH_3)_6$: A precursor for lithium niobate ceramics. Inorganic Chemistry 1990; 29(8): 1458-1459. https://doi.org/10.1021/ic00333a003
25. Wang S Y, Jiang H. Synthesis and characterization of $LiNbO_3$Powders by thermal decomposition method at low temperature. Ferroelectrics 2011; 413(1): 212–219. https://doi:10.1080/00150193.2011.554260
26. Khalameida S, Sydorchuk V, Leboda R, Skubiszewska-Zie¸ba J, Zazhigalov V. Preparation of nano-dispersed lithium niobate by mechanochemical route. Journal

of Thermal Analysis and Calorimetry 2014; 115:579–586. https://doi.org/10.1007/s10973-013-3343-5

27. Park S K, Koo S M, Lee Y E. Heterometallic lithium niobium complexes: Synthesis and molecular structures of $LiNbO(O\text{-}2,6\text{-}PhMe_2)_4 \cdot 3THF$ and $[LiNbCl_3(O\text{-}2,6\text{-}PhMe_2)_2 \cdot 2THF]_2$. Polyhedron 2000; 19(9): 1037-1041. https://doi.org/10.1016/S0277-5387(00)00341-7
28. Boyle T J, Alam M, Dimos D, Moore G J, Buchheit C D et al. Niobium(V) alkoxides synthesis, structure, and characterization of $[Nb(\mu\text{-}OCH_2CH_3)(OCH_2C(CH_3)_3)_4]_2$, $\{[H_3CC(CH_2O)(CH_2\text{-}\mu\text{-}O)(C(O)_2)]Nb_2(\mu\text{-}O)(OCH_2CH_3)_5\}_2$, and $\{[H_3CC(CH_2O)_2(CH_2\text{-}\mu\text{-}O)]Nb(OCH_2CH_3)_2\}_2$ for production of mixed metal oxide thin films. Chemistry of Materials 1997; 9: 3187-3198. https://doi.org/10.1021/cm970506p
29. Park S K, Park J W, Koo S M. The synthesis and thermal behavior of a heterometallic molecular precursor for lithium niobate. Journal of Ceramic Processing Research 2001; 2(1): 21-26.
30. Sharma M, Sharma M and Sharma N 2017 Physicochemical, quantum mechanical and thermoanalytical investigations of newly synthesized pentakis(2,4-dimethylphenoxo) niobium (V) as potential precursor of Nb_2O_5. Arabian Journal of Chemistry 2019; *12*(8): 5268-5277. http://dx.doi.org/10.1016/j.arabjc.2016.12.005
31. Sharma N, Pathania A, Sharma M. Thermoanalytical investigations of niobium (V) complexes of 4-isopropylphenol. Journal of thermal analysis and calorimetry 2012; 107: 149-154. https://doi.org/10.1007/s10973-011-1709-0
32. Sharma N, Sharma M, Bhatt S S, Chaudhry S C. Synthesis, characterization, and acceptor behavior of dichlorotris (2-t-butylphenoxo) niobium (V). Journal of

Coordination Chemistry 2010; 63: 680-687. https://doi.org/10.1080/00958971003615188

33. Sharma M, Pathania A, Sharma M, Sharma N. Niobium (V)-2-ethylphenoxide complexes: Synthesis, characterization and density functional theory calculations. Adv. Sci. Eng. Med. 2017; 9(3): 247-253. https://doi.org/10.1166/asem.2017.1982
34. Malhotra K C, Banerjee U K, Chaudhry S C. Reactions of phenoxides of niobium (V) and tantalum (V) with acetophenone and benzophenone. Acta Ciencia Indica-Chemistry 1980; 6(4): 236-238.
35. Liu M, Xue D, Luo C. Wet chemical synthesis of pure $LiNbO_3$ powders from simple niobium oxide Nb_2O_5. Journal of Alloys and Compounds 2006; 426(1): 118-122. https://doi.org/10.1016/j.jallcom.2006.02.019
36. Zhao J P, Liu X R, Qiang L S. Characteristics of the precursors and their thermal decomposition during the preparation of $LiNbO_3$ thin films by the Pechini method. Thin Solid Films 2006; 515(4): 1455-1460. https://doi.org/10.1016/j.tsf.2006.04.013
37. Niederberger M, Pinna N, Polleux J, Antonietti M. A general soft-chemistry route to perovskites and related materials: synthesis of $BaTiO_3$, $BaZrO_3$ and $LiNbO_3$ nanoparticles. Angewandte Chemie. 2004; 43(17): 2270-2273. https://doi.org/10.1002/ange.200353300
38. Luo C and Xue D. Mild, quasireverse emulsion route to submicrometer lithium niobate hollow spheres. Langmuir 2006; 22(24): 9914-9918. https://doi.org/10.1021/la062193v

39. Liu M and Xue D. A solvothermal route to crystalline lithium niobate. Materials Letters 2005; 59(23): 2908-2910. https://doi.org/10.1016/j.matlet.2005.04.041
40. Chien C H, Chang Y H, Tsai C P, Peng C W, Wang L S et al. Tetrahydrofuran activation assisted synthesis of nanosized lithium niobate and lithium tantalite. Journal of the Chinese Chemical Society 2006; 53: 287-292. https://doi.org/10.1002/jccs.200600035
41. Simoes A Z, Zaghete M A, Stojanovic B D, Riccardi C S, Ries A et al. $LiNbO_3$ thin films prepared through polymeric precursor method. Materials Letters 2003; 57(15): 2333-2339. https://doi.org/10.1016/S0167-577X(02)01221-1
42. Debnath C, Kar S, Verma S, Bartwal K S. Synthesis of $LiNbO_3$ nanoparticles by citrate gel method. Journal of Nanoscience and Nanotechnology 2015; 15(5): 3757-3763. https://doi.org/10.1166/jnn.2015.9769
43. Lanfredi S, Folgueras-Domingueza S, Rodrigues A C M. Preparation of $LiNbO_3$ powder from the thermal decomposition of a precursor salt obtained by an evaporative method. Journal of Materials Chemistry 1995; 5: 1957-1961. https://doi.org/10.1039/JM9950501957
44. An C, Tang K, Wang C, Shen G, Jin Y, Qian Y. Characterization of $LiNbO_3$ nanocrystals prepared via a convenient hydrothermal route. Materials Research Bulletin 2002; 37(11): 1791-1796. https://doi.org/10.1016/S0025-5408(02)00869-3
45. Camargo E R, Kakihana M. Low temperature synthesis of lithium niobate powders based on water-soluble niobium malato complexes. Solid State Ionics 2002; 151(1): 413-418. https://doi.org/10.1016/S0167-2738(02)00547-7

46. Khalameida S, Sydorchuk V, Leboda R, Skubiszewska-Zięba J, Zazhigalov V. Preparation of nano-dispersed lithium niobate by mechanochemical route. Journal of Thermal Analysis and Calorimetry 2014; 115(1): 579-586. https://doi.org/10.1007/s10973-013-3343-5
47. Puyôo-Castaings N, Duboudin F, Ravez J. Elaboration of $LiNbO_3$ ceramics from sol–gel process powders. Journal of Materials Research 1988; 3(3): 557-560. https://doi.org/10.1557/JMR.1988.0557
48. Rao A V P, Paik D S, Komarneni S. Sol-gel synthesis of lithium niobate powder and thin films using lithium 2, 4-pentanedionate as lithium source. Journal of Electroceramics 1998; 2(3): 157-162. https://doi.org/10.1023/A:1009918715122
49. Hirano S, Kato K. Formation of $LiNbO_3$ films by hydrolysis of metal alkoxides. Journal of Non-Crystalline Solids 1988; 100(1-3): 538-541. https://doi.org/10.1016/0022-3093(88)90079-8
50. Patterson A L. The Scherrer formula for X-Ray particle size determination. Physical Review 1939; 56: 978. https://doi.org/10.1103/PhysRev.56.978
51. https://imagej.nih.gov/ij/index.html
52. Anderson C. Dielectrics. London: Chapman & Hall 1964.
53. Khatri P, Behera B, Srinivas V, Choudhary R N P. Structural and dielectric properties of $Ba_3V_2O_8$ ceramics. Current Applied Physics 2009; 9(2): 515-519. https://doi.org/10.1016/j.cap.2008.05.002
54. Hyun K S, Su J M, Gyu C B, Suk Y Y. A study of dielectric properties of amorphous ferroelectric $LiNbO_3$. Journal of Korean Physical Society 1988; 32: S807-S810.

55. Hyun K S, Yoon-Hwae H, Jung-Ae K, Suk Y Y, Gyu C B et al. Study of frequency dependent ε*(ω) in amorphous ferroelectrics: Modified generalized Langevin equation analysis. Journal of Applied Physics 1999; 85: 347-351. https://doi.org/10.1063/1.369454

56. Cena C R, Behera A K, Behera B. Structural, dielectric, and electrical properties of lithium niobate microfibers. Journal of Advanced Ceramics 2016; 5(1): 84-92. https://doi.org/10.1007/s40145-015-0176-7

57. Barik R, Satpathy S K., Behera B.; Biswal, Susanta K.; Mohapatra R K.. Synthesis and spectral characterizations of nano-sized lithium niobate ($LiNbO_3$) ceramic. Micro and Nanosystems 2020; 12(2): 81-86. https://doi.org/10.2174/1876402911666190617114003

1 **Table1. Preparative methods of $LiNbO_3$ from different precursors**

Method	**Precursors**	**Crystal specifics**	**Ref.**
Non-aqueous	$Nb(OC_2H_5)_5$, Lithium	20-60 nm, PD, prismlike crystals, independent	45
Quasireverse emulsion	Nb_2O_5, $LiOH.H_2O$ in the presence of CTAB or SDS	100 nm PC, MD hollow spheres	46
Solvothermal	Nb_2O_5, Li_2CO_3	0.4-2.1 μm cubic shaped crystals	47
THF activation assisted	$NbCl_5$, Ethyllithium	20-50 nm lightly aggregated, spherical particles	48

Sol-gel (Low temperature)	1. $NbCl_5$ and LiOAc* Ac*= acetate	40-60 nm spherical crystals lightly fused 100-200 nm at higher temperature	17
Sol-gel (Pechinni method)	1. Nb_2O_5, Li_2CO_3, citric acid, ethylene glycol 2. $NbCl_5$, $LiNO_3$ and citric acid 3. Nb_2O_5, $LiNO_3$ and citric acid	70-100 nm highly fused crystal ~40 nm spherical particles ~87 nm	49 18 50
Thermal decomposition	1. $NH_4H_2[NbO(C_2O_4)_3]$ and $LiNO_3$ 2. $LiNbO(OC_6H_3\text{-}(CH_3)_2\text{-}2,6)_6]$	88 nm fused crystals 40-50 nm fine	51 28

		crystalline grains	
Hydrothermal	1. Nb_2O_5, LiOH 2. Nb_2O_5, $LiOH.H_2O$ or $LiNO_3$	40-100 nm flake like shape 2-4 μm hexahedron crystals	52 20
Wet-chemical	1. $Nb_2O_5.5H_2O$, Li_2CO_3, malic acid, oxalic acid and NH_3 solution 2. $Nb(OH)_5$, malic acid, NH_3 solution	…… 150 nm hexahedron shape	53 21
Mechanochemical method	Nb_2O_5 and Li_2CO_3	10-20 nm weakly aggregated	54
Hydrolysis and polycondensation method	Li(OEt) and $Nb(OEt)_5$	52-100 μm	55
Sol-gel (Metal-organic route)	Lithium2,4-pentanedionate, $Nb(OEt)_5$ and 2-methoxyethanol	……	56

Thermal decomposition	[LiNb($OC_6H_3Me_2$-2,4)$_6$]	54 nm	This study

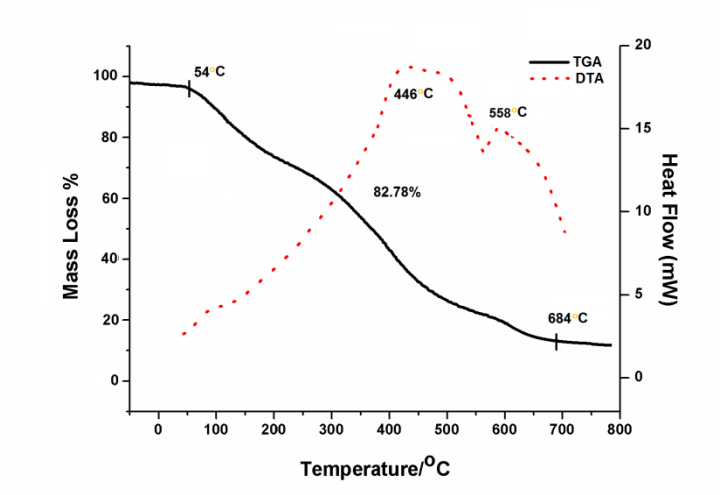

Figure 1. TG-DTA curve of [LiNb($OC_6H_3Me_2$-2,4)$_6$]

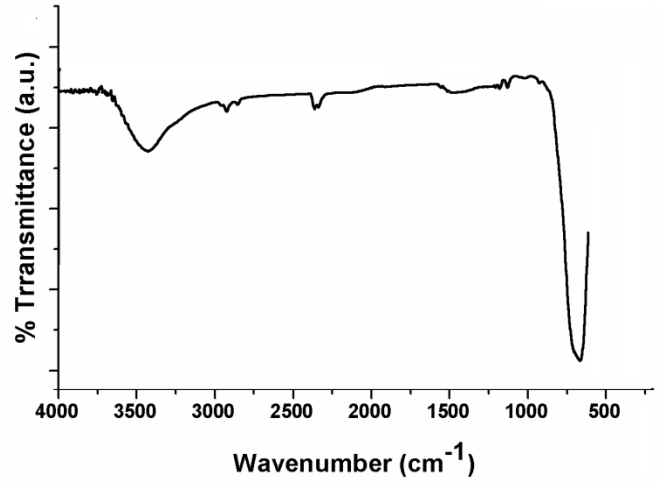

Figure 2. IR spectrum of $LiNbO_3$ nanopowders

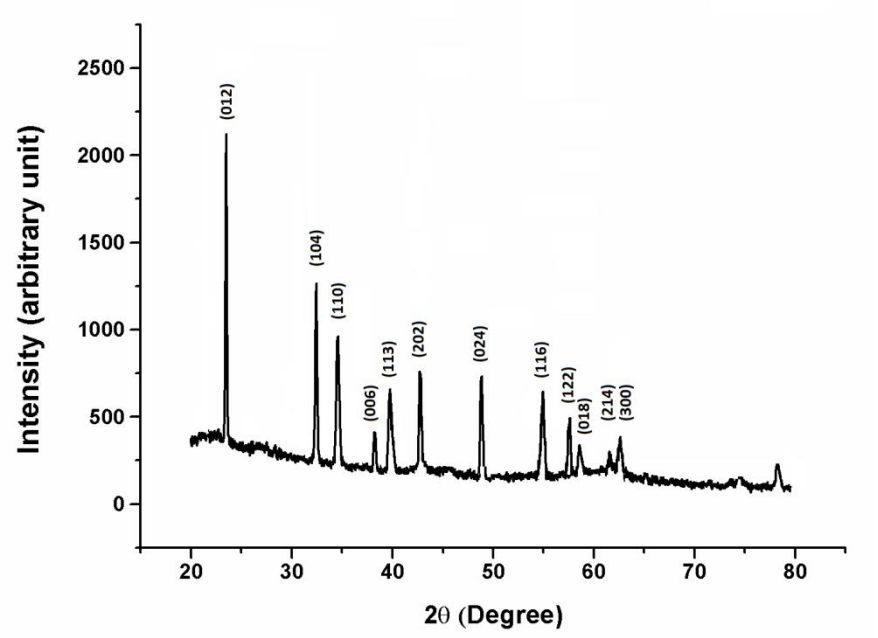

Figure 3. XRD pattern of $LiNbO_3$ nanopowders

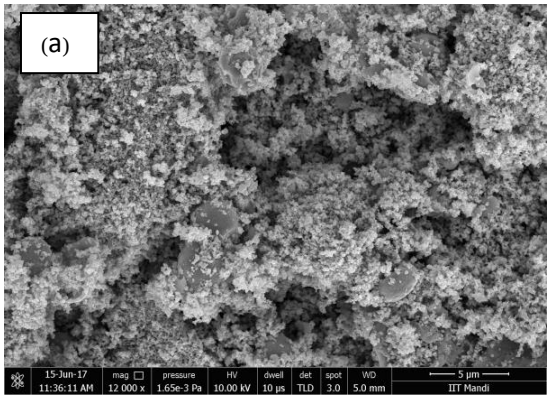

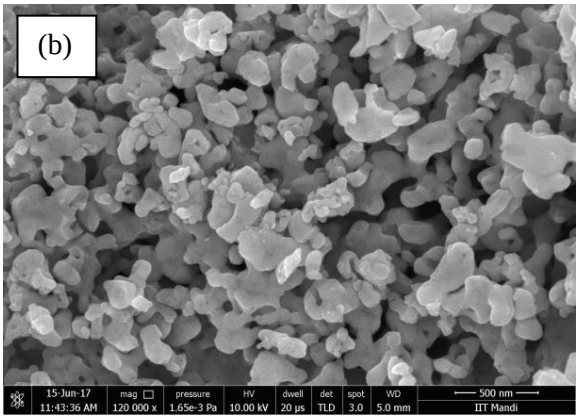

Figure 4. SEM images of LiNbO3 nanopowders with magnification of (a) 12000× and (b) 120000×

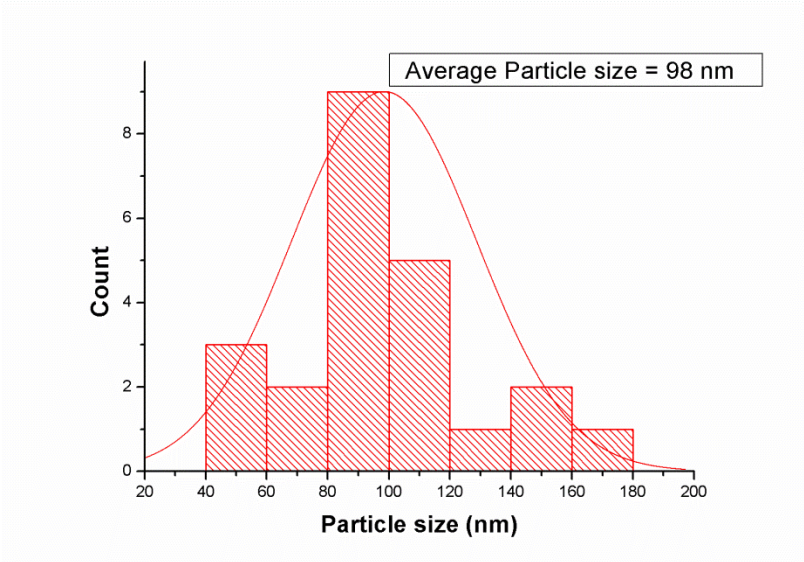

Figure 5. Particle size distribution of $LiNbO_3$ nanoparticles using ImageJ software

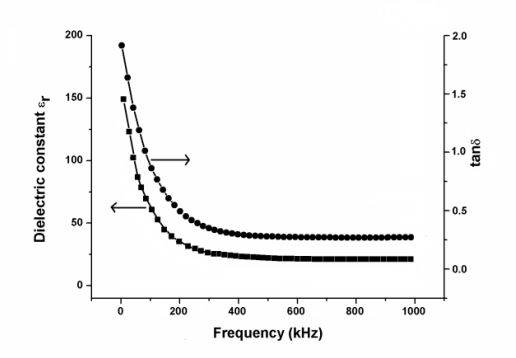

Figure 6. Variation of dielectric constant (ε_r) and loss tangent (tan δ) with frequency for $LiNbO_3$ nanopowder at room temperature

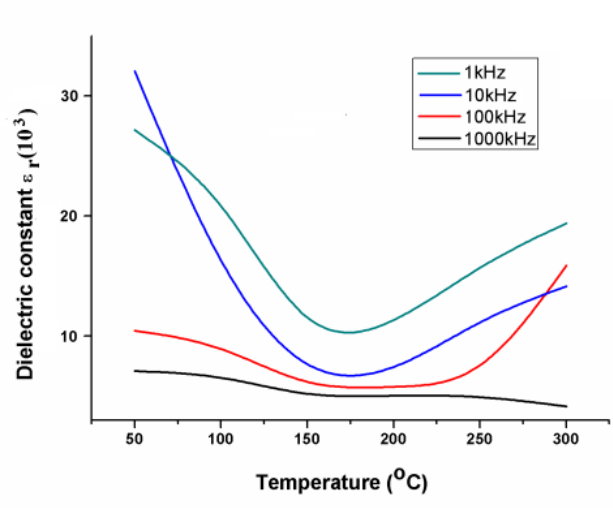

Figure 7. Variation of dielectric constant (ε_r) as a function of temperature of as obtained $LiNbO_3$ nanopowder at different frequencies

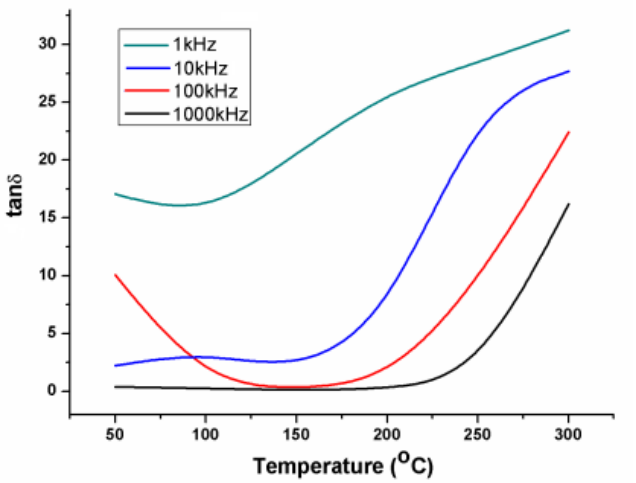

Figure 8. Variation of loss tangent (tan δ) as a function of temperature of $LiNbO_3$ nanopowders at different frequencies